

Influence of Strain Rate, Microstructure and Chemical and Phase Composition on Mechanical Behavior of Different Titanium Alloys

P.E. Markovsky and V.I. Bondarchuk

(Submitted December 21, 2016; in revised form April 12, 2017; published online June 14, 2017)

Taking three titanium commercial alloys: commercial purity titanium (c.p.Ti), Ti-6-4 (Ti-6(wt.%)Al-4V) and TIMETAL-LCB (Ti-1.5Al-4.5Fe-6.8Mo) as program materials, the influence of phase composition, microstructure and strain rate (varied from 8×10^{-4} to 1.81×10^{-1}) on the mechanical behavior was studied. The size of the matrix phase (α - or β -grains) and size of $\alpha + \beta$ intragranular mixture were varied. Such parameter such as tensile toughness (TT) was used for analysis of the mechanical behavior of the materials on tension with different rates. It was found that the TT values monotonically decreased with strain rate, except Ti-6-4 alloy with a globular type of microstructure. In single-phase α -material (c.p.Ti), tensile deformation led to the formation of voids at the intragranular cell substructure, and merging of these voids caused the formation of main crack. In two-phase $\alpha + \beta$ materials, the deformation defects were localized upon tension predominantly near the α/β interphase boundaries, and subsequent fracture had different characters: In Ti-6-4 globular condition fracture started by formation of voids at the α/β interphase boundaries, whereas in all other conditions the voids nucleated at the tips of α -lamellae/needles.

Keywords mechanical properties, mechanical behavior, microstructure, strain rates, tensile toughness, tension tests, titanium alloys

1. Introduction

The titanium alloys are a unique class of structural materials for many applications, and first of all— aerospace and military, due to their high specific strength, fatigue endurance, crack growth and corrosion resistances (Ref 1-3). In some cases, these materials are employed in parts working at high stresses and tough operating conditions, particularly in parts subjected to high-rate deformations and high strengths. For instance, similar service conditions will take place upon operations of aircrafts' landing gears and all types of supersonic aircrafts, including the new generation of civil ones (Ref 4, 5), as well as in a wide range of products for military use (Ref 6, 7). Unfortunately, there are scarce data in the literature on the behavior of titanium alloys under these conditions. The effect of strain rate on the mechanical properties of some alloys in coarse-grained metastable β states was studied in (Ref 8, 9). In our previous work, we investigated the influence of β -grain size, crystallographic texture and presence of strengthening α -particles on the mechanical behavior of several high-strength metastable β titanium alloys (Ref 10-12). At the same time, aerospace designers now demand for a new strength level above 1500 MPa for such titanium parts as fasteners, springs and chassis components, which usually work below the yield

stress. However, as it was shown by our previous studies (Ref 11, 12), such high-strength states do not provide a sufficiently high level of tensile toughness [TT, also known as deformation energy (U_T) (Ref 13)] under loading with high rates that may take place under emergency conditions. Since these results were obtained only for titanium alloys of metastable β class in two structural conditions, namely single-phase β and aged high-strength $\alpha + \beta$, it was principally important to establish the influence of strain rate during deformation on the mechanical behavior of another widely used commercial titanium alloys, first of all α and $\alpha + \beta$ types. Also, it was important to clarify the role of microstructure in these processes. The present work was focused on answering these questions.

2. Materials and Experimental Procedures

Three different commercial titanium alloys were chosen as program materials: commercial purity titanium (c.p.Ti), the “working horse” of titanium industry two-phase alloy Ti-6(wt.%) Al-4V and high-alloyed metastable β -alloy TIMETAL-LCB (Ti-1.3Al-4.5Fe-6.8Mo). All alloys were received in the form of rod with the following diameters: 18 mm (c.p.Ti), 14 mm (Ti-6-4) and 12 mm (LCB). These rods were cut in a way to obtain six batches of specimens (55 mm long each) which were subjected to heat treatments listed in Table 1. The heat treatments #1, 3 and 6 (annealing) were aimed on stabilization of the initial phase composition and microstructure in studied materials. In c.p.Ti obtained after annealing microstructure was characterized by relatively fine equiaxed α -grains (Fig. 1a), while in Ti-6-4—coexistence of primary α -globules and fine β -crystals between them (Fig. 1c). Other heat treatments were performed to form another types of microstructure, namely: #2—with coarser α -phase (Fig. 1b), #4—with microstructure of bimodal type, wherein instead of initial

P.E. Markovsky and V.I. Bondarchuk, G.V. Kurdyumov Institute for Metal Physics, National Academy of Sciences of Ukraine, 36, Vernadsky Blvd., Kiev 03142, Ukraine. Contact e-mail: pmark@imp.kiev.ua.

Table 1 Program alloys, applied treatments and obtained microstructural states

##	Alloy	Treatment	Designation	Microstructure type	Microstructure features, μm	
					α -Phase size	β -Phase size
1	c.p.Ti	800 °C, 1 h, cooling 5 °C/min	cpTiFG	Equiaxed finer	Average diameter ~ 80	...
2	c.p.Ti	950 °C, 1 h, cooling 5 °C/min	cpTiCG	Equiaxed coarser	Average diameter ~ 200	...
3	Ti-6Al-4V	800 °C, 1 h, cooling 10 °C/min	Ti64GL	Globular	Primary: Average diameter ~ 2	Particles with average size $\sim 0.2-0.5 \times 1-3$
4	Ti-6Al-4V	880 °C, 1 h, water quenching + 700 °C, 1 h, cooling 10 °C/min	Ti64BM	Bimodal	Primary: Average diameter ~ 2 ; secondary: $\sim 0.5 \times 1.4$	Colonies with average size $\sim 0.1-0.4 \times 0.3-1.5$
5	Ti-6Al-4V	1100 °C, 1 h, cooling 10 °C/min	Ti64LM	β -transformed lamellar	Thickness of grain boundary ~ 10 ; intragrain ~ 8	Average β -grain size ~ 400 ; thickness of lamellae ~ 1
6	TIMETAL-LCB	700 °C, 1 h, cooling 10 °C/min	LCB	β -transformed lamellar	Thickness of grain boundary ~ 0.3 ; intragrain $\sim 0.1 \times 0.6$	Average β -grain size ~ 6

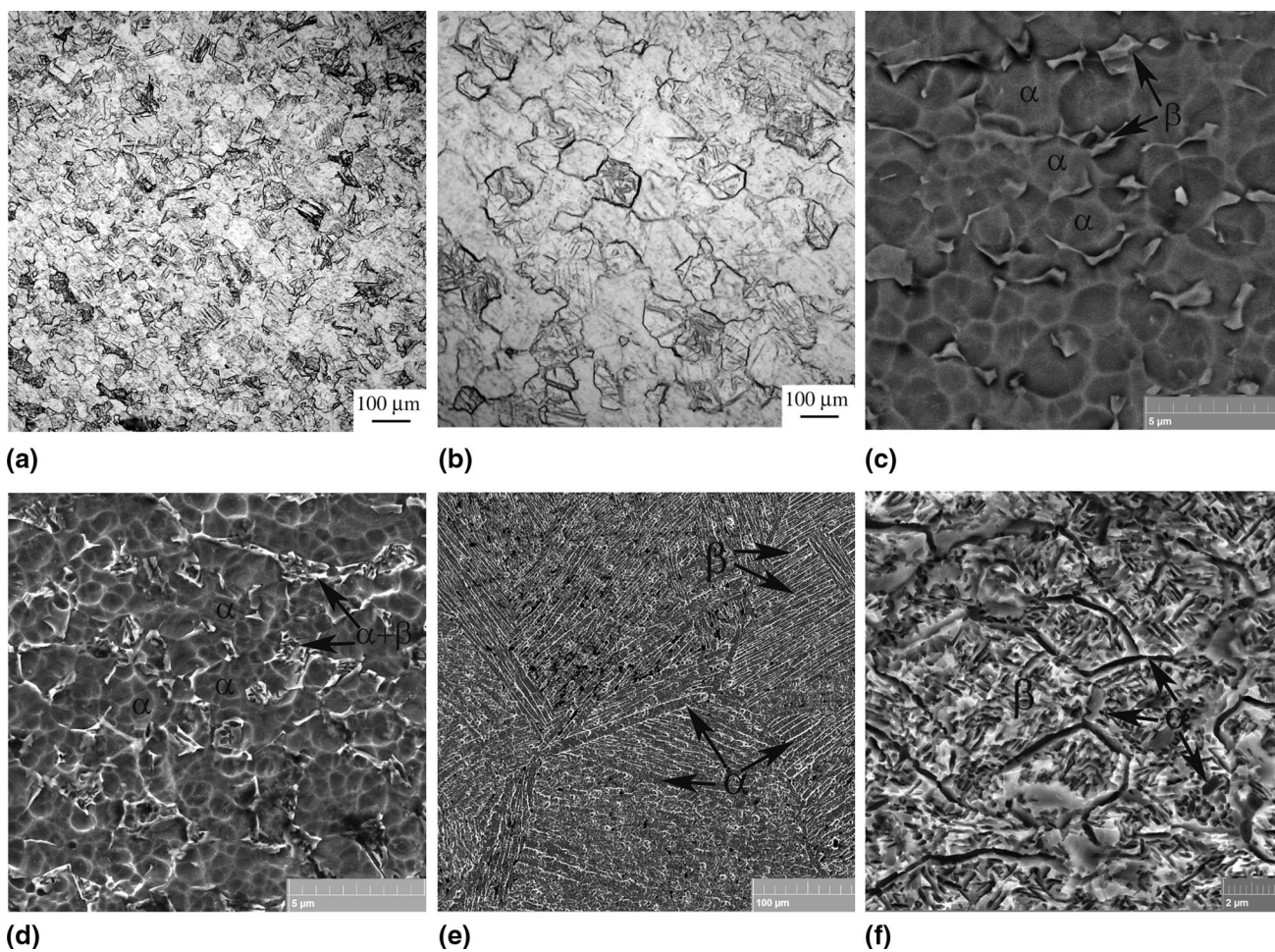


Fig. 1 Microstructure of program materials: (a) cpTiFG, (b) cpTiCG, (c) Ti64GL, (d) Ti64BM, (e) Ti64LM and (f) LCB. (a, b) LM; (c-f) SEM

β -phase appeared zones of β -transformed microstructure containing fine lamellae of α -precipitates (Fig. 1d), #5—with completely β -transformed microstructure characterized by coarse β -grains and large packets of α -lamellae inside with

very fine layers of β -phase between α -lathes (Fig. 1e). Concerning the microstructure of LCB formed upon annealing (heat treatment #6), it should be mentioned that it is a result of α -phase precipitation in relatively fine-grained β -structure

obtained evidently during dynamic recrystallization under hot rolling at high temperatures near the beta-transus [T_β —temperature of finishing of $\alpha + \beta_0 \rightarrow \beta$ polymorphous transformation (Ref 2, 14)].

The microstructure was examined with standard light, scanning and transmission electron microscopy (LM, SEM and TEM, respectively) in the initial and deformed conditions. Phase composition was determined with x-ray diffraction analysis. The tensile specimens with gage of 4 mm diameter and 25 mm length were machined and tested in accordance with the ASTM E8M standard for all conditions. Tensile tests were carried out at INSTRON-3376 unit. Basing on the results of previous studies (Ref 10-12), we chose four strain rates: 8.00×10^{-4} , 4.00×10^{-3} , 3.62×10^{-2} and 1.61×10^{-1} . Also it should be noted that peak temperature of specimens strained even with higher rate 3.6×10^{-1} was not exceeded 90-105 °C (Ref 10) (heating as a result of intensive plastic deformation); therefore, this factor can be neglected in the present study. Tensile toughness [TT, or deformation energy (Ref 13)] was calculated for every studied state on the base of results obtained for three specimens for each strain rate. Fracture surfaces of tested specimens, as well as details of deformed state nearby fractured surfaces, were examined with SEM and in the last case on the samples cut and polished in longitudinal direction

along tensile axis as it is shown in Fig. 2(a). After that, foils for TEM study were cut and electrolytically polished. Integral and local chemical compositions of the fractured and polished surfaces of specimens were studied at SEM equipped with EDS analysis system.

3. Experimental Results and Discussions

3.1 Single-Phase α -(hcp) Alloy (c.p.Ti)

Typical engineering stress-strain curves of two types of commercial purity titanium specimens that differ in the size of equiaxed α -grains (Fig. 1a and b; #1 and 2 in Table 1) are presented in Fig. 3. The curves are dome shaped at all strain rates. As can be concluded from analysis and comparison of Fig. 3(a) and (b), general tendency for tensile properties of these materials is rather common—increase in strain rate causes some decrease in elongation and a little increase in strength. The differences in mechanical behavior between these two microstructural states of c.p. Ti were insignificant. As a result, the dependencies of tensile toughness on strain rate were rather similar (Fig. 4).

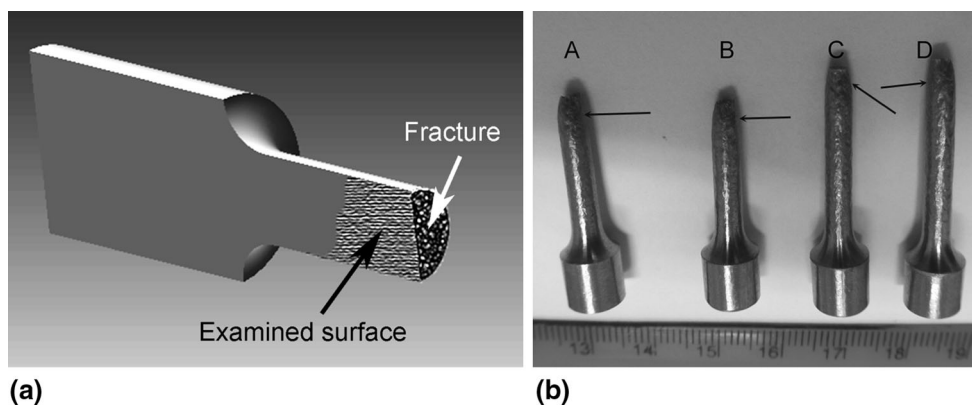


Fig. 2 (a) Scheme illustrating preparation of specimens for SEM and TEM studies; (b) general view of cpTiFG specimens tested with strain rates: (A) 8.00×10^{-4} ; (B) 4.00×10^{-3} ; (C) 3.62×10^{-2} ; and (D) 1.81×10^{-1} . Arrows show locations where disks for TEM study were cut

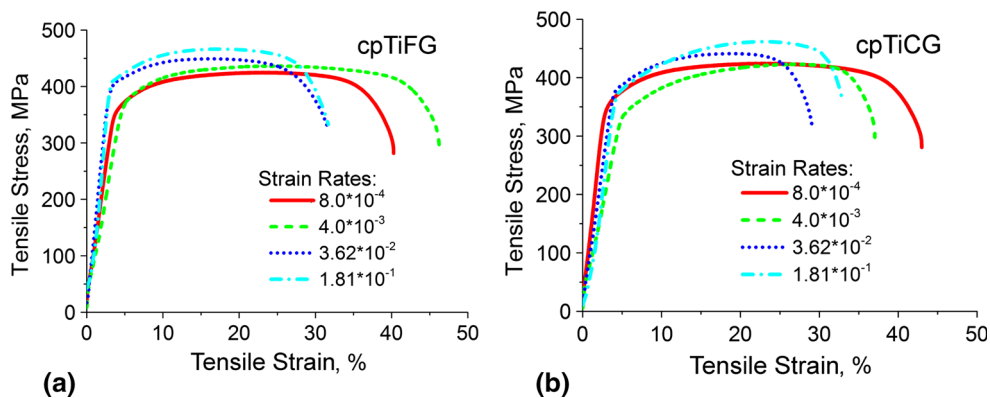


Fig. 3 Typical engineering tensile stress-strain curves of (a) cpTiFG and (b) cpTiCG tested with different strain rates

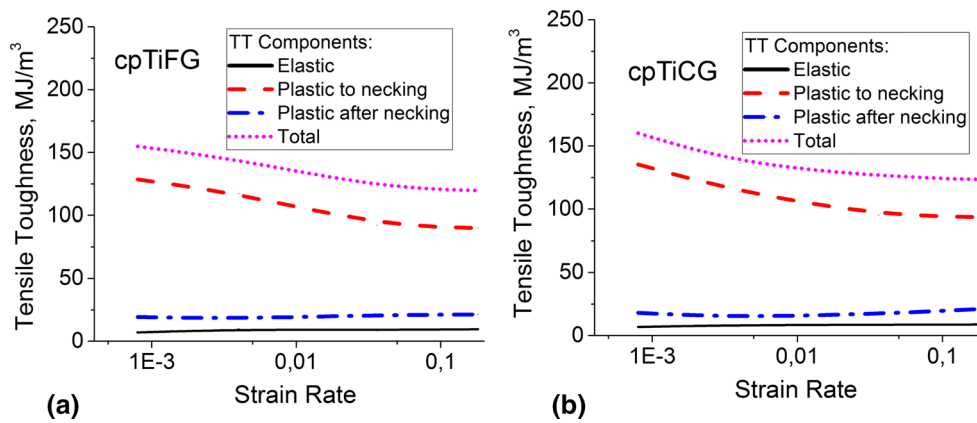


Fig. 4 Tensile toughness of (a) cpTiFG and (b) cpTiCG states tested with different strain rates

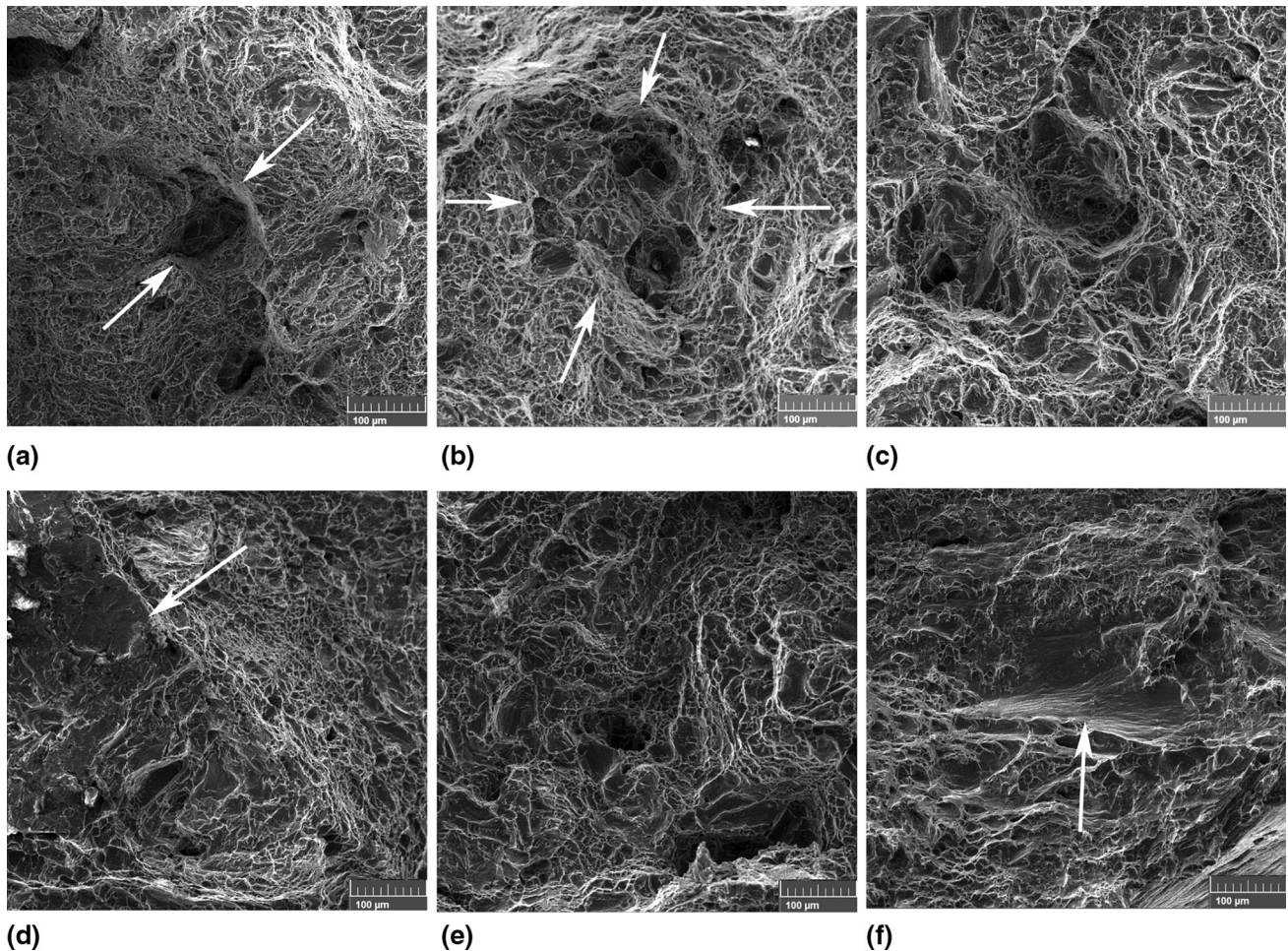


Fig. 5 Typical fracture surfaces of c.p.Ti in (a, c, e) cpTiFG and (b, d, f) cpTiCG states tested with strain rates: (a, b) 8.00×10^{-4} , (c, d) 3.62×10^{-2} , (e, f) 1.81×10^{-1} . SEM. Arrows indicate: (a) α -grain contour; (d, f) cracks propagation along α -grain boundary

It is important to note that, despite the increase in strain rate, the input of separate different TT components into total one (Fig. 4) remains the same for all studied strain rates. In other words, only plastic deformation component gradually decreased, whereas two other components remained actually on the same level (Fig. 4). Also it is worthwhile to mention that traces of plastic flow were seen over the entire lateral surface of

fractured specimens (Fig. 2b), that indicates on the development of uniform plastic deformation through the whole volume of the samples even at the highest strain rate.

Typical examples of fracture surfaces of cpTiFG and cpTiCG are shown in Fig. 5. It is seen that both microstructural types for all straining rates are characterized by ductile character of fracture. Regardless of strain rate, the size of

ductile dimples in both materials varied within the range of 8–15 μm . Taking into account that the size of initial α -grains was essentially different (80 and 200 μm for cpTiFG and cpTiCG, respectively—see Fig. 1a and b; ##1 and 2 in Table 1), it is possible to conclude that the formation of voids (voids) was not related to the grain boundaries, and evidently they were initiated at intragrain substructure which readily develops in this material during plastic deformation (Ref 15). This allows to assume that the nucleation of voids and cracks is not associated with high-angle α -grain boundaries. At the same time, some dished fragments are seen with size comparable to the size of α -grains (Fig. 5a, c and e). While for the cpTiFG state significant changes in fracture surface character with increase in strain rate were not observed, in cpTiCG separate flat areas appeared with strain rate increase (Fig. 5d and f). Taking into account that the size of these areas is rather close to the size of some grain boundaries (Fig. 1b), this fact can be related to crack propagation along these boundaries.

Typical microstructure of cpTi in the area of intensive deformation near the fracture surface is shown in Fig. 6. It is clearly seen that the plastic deformation leads to the transformation of initial equiaxed α -phase globules into the set of elongated along strain direction grains with a lot of voids (Fig. 6a) which are not related to microstructural elements

(Fig. 6b). In all examined locations, the smallest voids had size less than a few micrometers. Figure 6(c) shows that these voids grew and merged, forming eventually ductile dimples on the fracture surface.

Measurements of local chemical composition on various areas of fractured surface, as well as on the bottoms of dimples, did not show any visible enrichment in impurities, which would allow to suggest that the dimples were formed on dislocation tangles accompanied by Cottrell atmospheres. TEM study of fine microstructure in the zones located close to the fracture surfaces (see Fig. 2) showed that the substructure formed on straining had different nature (Fig. 7). For instance, it was found a number of relatively small cells (Fig. 7a) with dislocation loops inside (Fig. 7b), as well as a limited number of typical for h.c.p. titanium twins (Fig. 7c) (Ref 16). At the same time, it should be noted that the TEM images (for cpTi and other alloys studied) were obtained for locations at some distance (3–4 mm) from the fracture surface, because upon electropolishing pores and places with high concentration of defects were etched out too quickly, which did not allow to obtain high-quality foils. Nevertheless, these microstructures allow to illustrate the formation of substructure of alloy at the stage preceding the formation of pores. Comparison of such substructures formed on straining with different rates did not

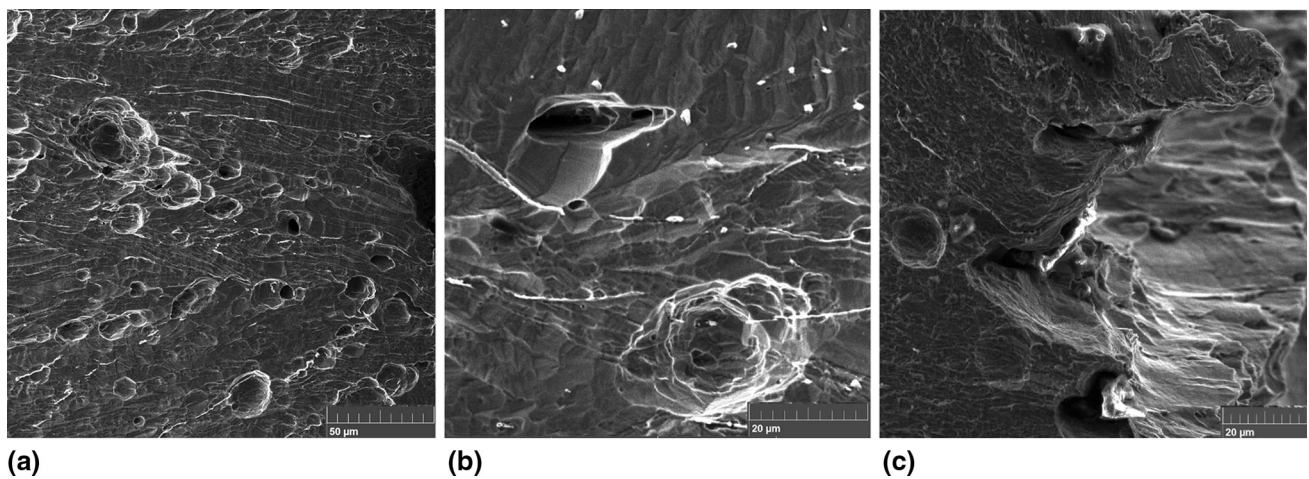


Fig. 6 Microstructure of cpTiCG specimen tested with strain rate 3.62×10^{-2} near the fracture surface polished in longitudinal direction. SEM

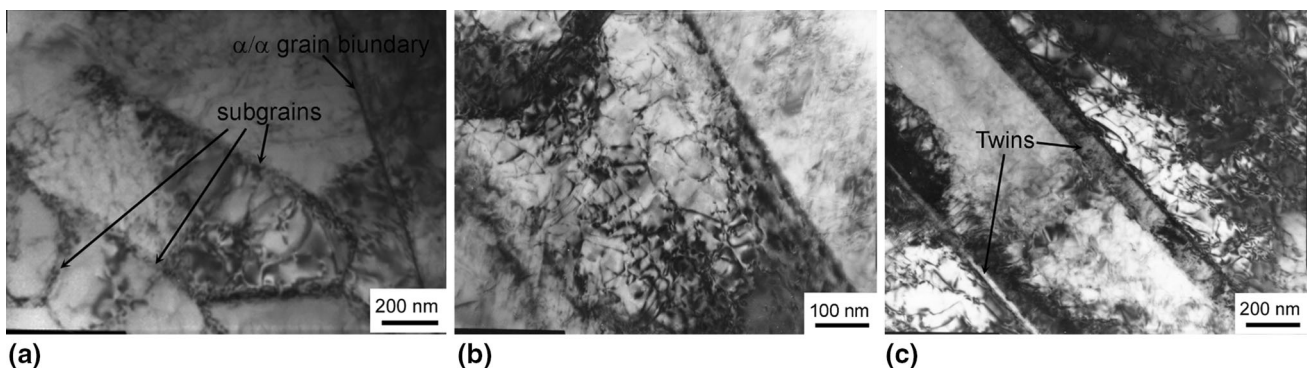


Fig. 7 Typical TEM images of cpTiCG specimens tested with strain rate (a) 3.62×10^{-2} and (b, c) 1.81×10^{-1} near the fracture surface. TEM

reveal noticeable differences. Probably, increase in strain rate caused in narrowing of the zone of localized deformation, in which the pores formed.

So, taking into account the above mentioned, it is possible to assume that, regardless of the α -grain size and strain rate, the void initiation, growth and merging may be associated with the formation of intragrain dislocation substructure, whereas the crack propagation at a sufficiently high strain rates and larger grain sizes can develop along some long grain boundaries in microstructure having coarser α -grains (Fig. 5d and f).

3.2 Low-Alloyed Two-Phase $\alpha + \beta$ Alloy Ti-6Al-4V

Unlike cpTi, the engineering stress-strain curves of Ti-6-4 alloy were characterized by a sharp transition from elastic to plastic deformation (Fig. 8). Ti64GL and Ti64BM states have very close characteristics of strength and ductility (Fig. 8a and b), whereas Ti64LM, as expected, was characterized by lower tensile properties (Fig. 8c). Strain rate increase caused visible reduction in elongation for all three microstructural states.

The TT data showed essential difference in strain rate dependencies (Fig. 9). First of all, it should be noted that in globular condition the material showed unusual very weak strain rate dependence of total TT, as well as its components (Fig. 9a). Two other microstructural states were more sensitive to strain rate mainly due to decrease in the plastic deformation to necking (Fig. 9b and c).

Figure 10 illustrates typical examples of fracture surfaces of Ti-6Al-4V alloy with different microstructures tested with various strain rates. First of all, it should be noted that two

conditions with globular primary α -phase, Ti64GL and Ti64BM, are characterized by completely ductile fracture after strain with all applied rates (Fig. 10a, b, c, e, f, h and i). The size of the majority of dimples corresponds to the size of initial α -globules; at the bottom of the dimples, a lot of voids are visible (Fig. 10b, c, f and h). The fracture surface of Ti64LM has principally different characters—it consists of two different areas: flat facets and relatively ductile regions with traces of lamellar packets (Fig. 10d, g and j).

Typical TEM microstructures of all studied states in Ti64 alloy (also observed on the distance 3-4 mm from the fracture edge) are presented in Fig. 11. In globular condition (Ti64GL), an increased density of dislocations was observed mainly nearby α/β boundaries, and the shape of separate α -particles changed from globular to faceted one (Fig. 11a). In bimodal condition (Ti64BM), an increased density of deformation defects was found predominantly in the secondary α -lamellas and β -layers between them (Fig. 11b). In the lamellar Ti64LM specimens, TEM study revealed localization of deformation defects mainly in α -lathes, whereas β -interlayers looked relatively free of defects (Fig. 11c). The principal difference in the deformation substructure of all these structural states with increasing strain rate was not detected, probably because investigated locations were at some distance from the hearth of the most intense deformation near the fracture surfaces.

Study of microstructure on longitudinal polished sections near the fracture surfaces revealed multiple voids formation in Ti64GL and Ti64BM materials (Fig. 12a-d). In the first case, this process can be associated with β -phase particles (or likely

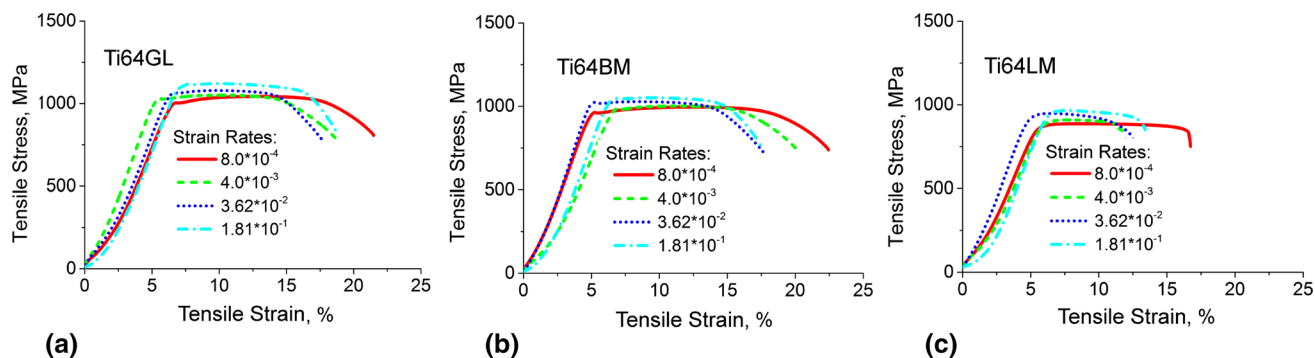


Fig. 8 Typical engineering tensile stress-strain curves of Ti-6Al-4V in (a) Ti64GL, (b) Ti64BM and (c) Ti64LM states tested with different strain rates

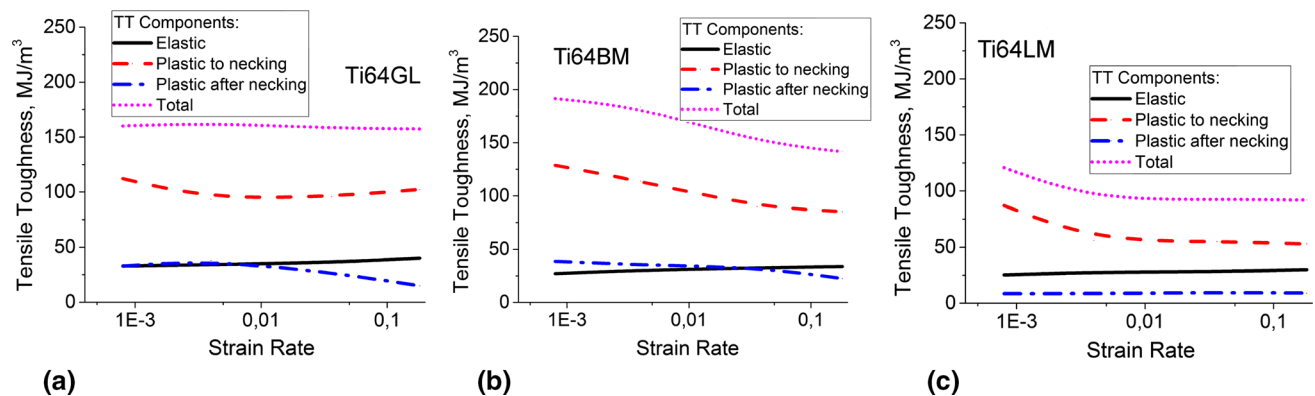


Fig. 9 Tensile toughness of Ti-6Al-4V in (a) Ti64GL, (b) Ti64BM and (c) Ti64LM states tested with different strain rates

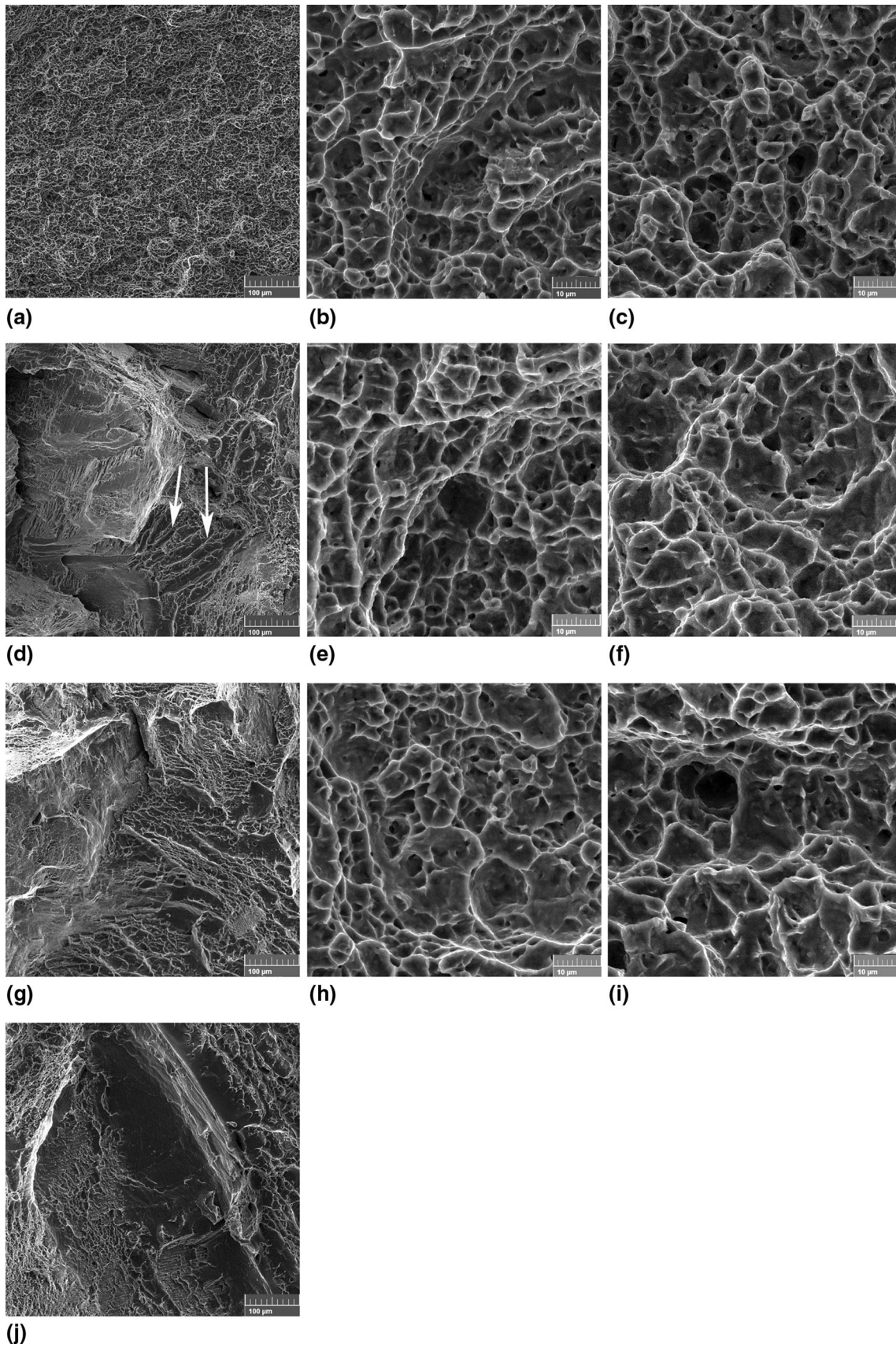


Fig. 10 Typical fracture surfaces of Ti-6-4 alloy in (a, b, e, h) Ti64GL, (c, f, i) Ti64BM and (d, j, j) Ti64LM conditions after tension with rates: (a-d) 8.00×10^{-4} , (e-g) 3.62×10^{-2} and (h-j) 1.81×10^{-1} . Arrows in (d) show traces of lamellar packets. SEM

with α/β interphase boundaries, Fig. 12b), whereas in the second case—with tips of fine secondary α -particles in the transformed β regions (Fig. 12d). In both cases, these particles were tilted and elongated in the direction of plastic flow. Strain rate influence appears in that fact that its increase reduced both the number of voids and the depth of the area where they form. In Ti64LM material, the number of voids is very restricted,

their appearance can be associated with the tips of α -lamellae inside the β -grains (Fig. 12f), and cracks can propagate along coarse α -lamellas coating β -grain boundaries (Fig. 12e), which evidently leads to the formation of facets on the fracture surfaces (Fig. 10d, g and j). These observations are in a good agreement with the data from a number of works, which established that spall in rapidly deformed Ti64 alloy occurs due

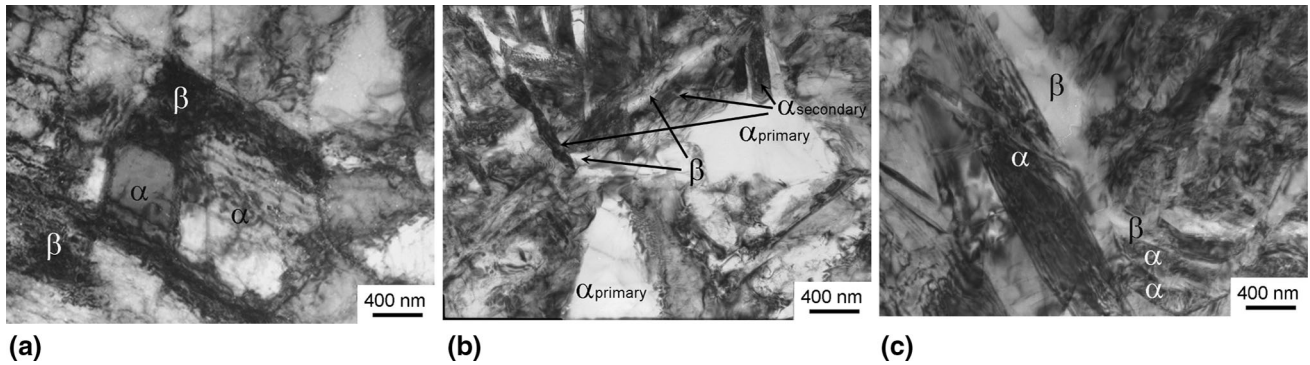


Fig. 11 Typical TEM images of (a) Ti64GL, (b) Ti64BM and (c) Ti64LM specimens tested with strain rate (a) 3.62×10^{-2} and (b, c) 1.81×10^{-1} near the fracture surface. TEM

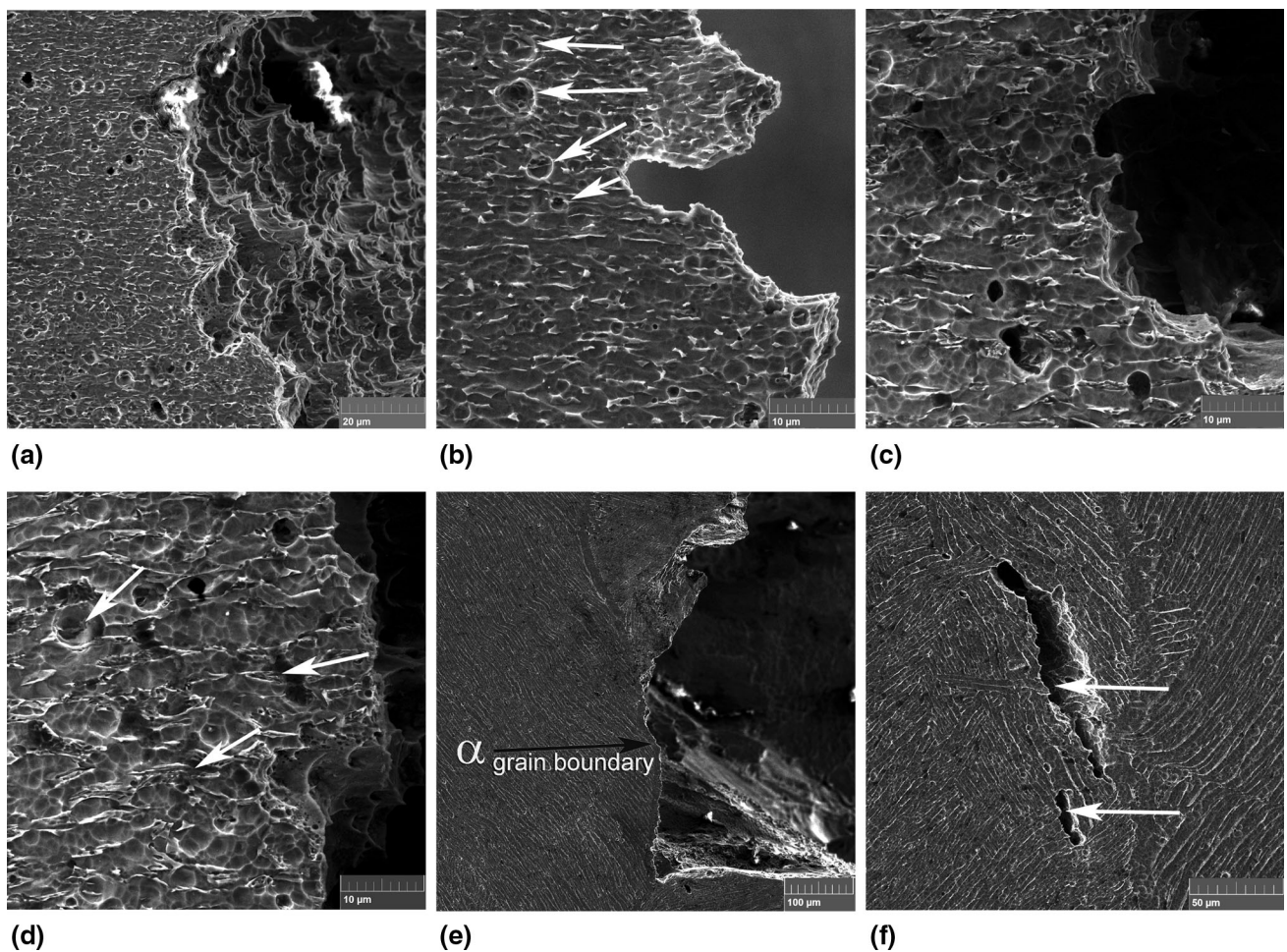


Fig. 12 Typical microstructure of Ti-6-4 specimens polished in longitudinal direction under the neck in different microstructural states tested with different strain rates: (a, b) Ti64GL, (c, d) Ti64BM, (e, f) Ti64LM. Arrows show: (b) voids initiated at α/β boundaries in Ti64GL; (d) voids initiated at fine α -precipitates in Ti64BM; (f) voids and crack initiated at coarse α -lamellae. SEM

Table 2 Local chemical compositions on fracture surfaces of Ti-6Al-4V alloy with different microstructures (two-phase $\alpha + \beta$ states)

##	Strain rate	Chemical composition, wt.%			Location
		Al	V	Fe	
Globular					
1	8.00×10^{-4}	5.09	3.37	NA	Ductile
2		7.83	3.43	NA	
3		5.16	3.30	0.39	
4		4.32	3.42	0.16	
5		6.09	3.39	0.50	
6		7.10	3.78	0.44	
Average		5.94	3.45	0.38	
7	3.62×10^{-2}	3.28	4.11	0.24	Ductile
8		5.61	4.14	0.44	
9		4.80	4.00	0.28	
10		5.21	8.11	1.47	
11		5.84	3.11	0.27	
12		4.74	3.06	0.27	
Average		4.91	4.42	0.50	
13	1.81×10^{-1}	6.56	3.61	0.53	Ductile
14		6.55	3.60	0.35	
15		6.45	4.96	0.62	
16		5.79	5.95	0.89	
17		6.08	4.29	0.54	
18		7.43	3.40	0.36	
Average		6.48	4.30	0.55	
Bimodal					
19	8.00×10^{-4}	4.57	5.18	0.72	Ductile
20		8.34	2.66	0.20	
21		6.65	2.74	0.31	
22		5.05	4.11	0.41	
23		5.40	3.20	0.27	
24		4.77	2.45	0.00	
Average		5.80	3.39	0.32	
25	3.62×10^{-2}	5.60	3.43	NA	Ductile
26		1.40	5.67	0.48	
27		7.57	3.65	NA	
28		1.90	4.92	NA	
29		3.56	4.34	NA	
30		7.19	5.33	0.70	
Average		4.54	4.56	0.59	
31	1.81×10^{-1}	6.86	4.47	0.34	Ductile
32		5.82	2.10	0.00	
33		4.61	2.43	0.00	
34		2.90	2.84	0.24	
35		5.92	2.49	0.00	
36		3.35	3.43	0.00	
Average		4.92	2.96	0.29	
Lamellar					
37	8.00×10^{-4}	7.64	3.89	0.43	Brittle
38		4.03	13.19	0.00	
39		6.96	5.00	0.37	
40		5.54	3.80	0.29	
41		7.54	3.75	0.25	
42		6.12	4.74	0.56	
Average		6.31	5.73	0.32	
43	3.62×10^{-2}	7.42	5.03	0.61	Brittle
44		7.28	4.51	0.46	
45		7.49	4.48	0.58	
46		5.21	4.47	0.38	
47		7.80	4.30	0.44	
48		4.27	3.60	0.48	

Table 2 continued

##	Strain rate	Chemical composition, wt. %			Location
		Al	V	Fe	
Average		6.58	4.40	0.49	
49	1.81×10^{-1}	5.05	3.87	0.39	Brittle
50		1.50	4.13	0.15	Brittle
51		4.77	9.92	1.72	Ductile
52		0.55	3.49	0.26	Brittle
53		6.79	3.09	0.28	Brittle
54		7.82	2.18	0.00	Brittle
Average		4.41	4.45	0.45	

Table 3 Local chemical compositions of Ti-6-4 alloy in different initial microstructural states

##	Average chemical composition, wt. %			Phase
	Al	V	Fe	
Ti64GL				
1	7.34	2.00	0.00	α
2	3.22	18.96	4.81	β
Ti64BM				
3	7.55	2.24	0.00	α
4	2.92	18.27	3.02	β
Ti64LM				
5	7.89	1.52	0.00	α
6	4.27	14.88	3.06	β

to the nucleation of voids at grain boundaries (as a result of localization of defects), followed by void growth and coalescence into facets and the subsequent coalescence of those facets in shear bands and cracks (Ref 17, 18). Also this corresponds to the scheme proposed in (Ref 19), which illustrates the evolution of substructure during high-strain deformation of Ti-6Al-4V alloy.

Local chemical compositions of the fractured surfaces of Ti-6Al-4V alloy in three different microstructural states are listed in Table 2. In the case of totally ductile fracture of Ti64GL, the chemical composition on various sites was very close to the nominal one (except some points: ##2, 4, 7 and 18), and there was no difference for different strain rates. In Ti64BM specimens, a wider scatter of local composition was observed—for instance, aluminum content varied from 1.40 to 7.19 wt.%, and vanadium content varied from 2.10 to 5.33 wt.%. In Ti64LM material, the scatter of local chemical composition became much higher: Aluminum content changed from 1.50 to 7.64 wt.% and vanadium—from 3.49 to 13.19 wt.%. The largest scatter in alloying elements content corresponds to the brittle areas of fracture surfaces, whereas in ductile areas it is rather similar to the above cases of globular and bimodal microstructures (compare ##39, 42, 48 and 51 with ##1-36 in Table 2).

To explain these data, we have to consider the results of the analysis of chemical composition of this alloy on flat samples (Table 3), and the general character of alloying elements redistribution in α - and β -phases (Fig. 13). As shown in Fig. 13(a) and (b) and pp. ##1 and 2 in Table 3, the β -alloying elements (vanadium and iron) are allocated predominantly in β -phase, while aluminum—in α -phase. The boundary between α -

and β -phases is clearly seen and rather sharp [within the limits of EDS accuracy (Ref 20)]. Comparing the data presented in Tables 2 and 3 and keeping in mind the foregoing discussion on the microstructure influence on fracture, it is possible to assume that voids and then rupture dimples form predominantly near the α/β interphase boundaries, where the content of alloying elements is close to the nominal composition of the alloy.

As for Ti64BM material, the situation looks very similar to the Ti64GL, except the fact that by the concentration profiles it is impossible to distinguish accurately α - and β -phases compositions inside the β -transformed regions which consist of fine lamellar $\alpha + \beta$ mixture (Fig. 13c and d). As the data shown in Table 2 (p 19–36) and Table 3 (p 3 and 4), for this microstructural state it also can be assumed that fracture occurred predominantly at α/β interphase boundaries, but it is difficult to assert the type of these boundaries—whether they are between the primary α -phase globules or within the β -transformed zones (i.e., between the α - and β -lamellae). However, taking into account the size of dimples which is close to the diameter of primary α -globules, the first version looks more preferable. At the same, as it was noted above, formation of pore was found near the tips of fine particle of secondary α -phase (Fig. 12d). Taking into account these, two points become possible to assume that tips of secondary α -particle nucleate initial pores, but then their growth reaches the interfaces with the primary α -globules and after intensive propagation along these interfaces finally forms dimples on fracture surface.

The fracture of Ti64LM material is characterized by pronounced features. In the regions of brittle fracture, chemical composition varies widely—for instance, in zone p 38 (Table 2)

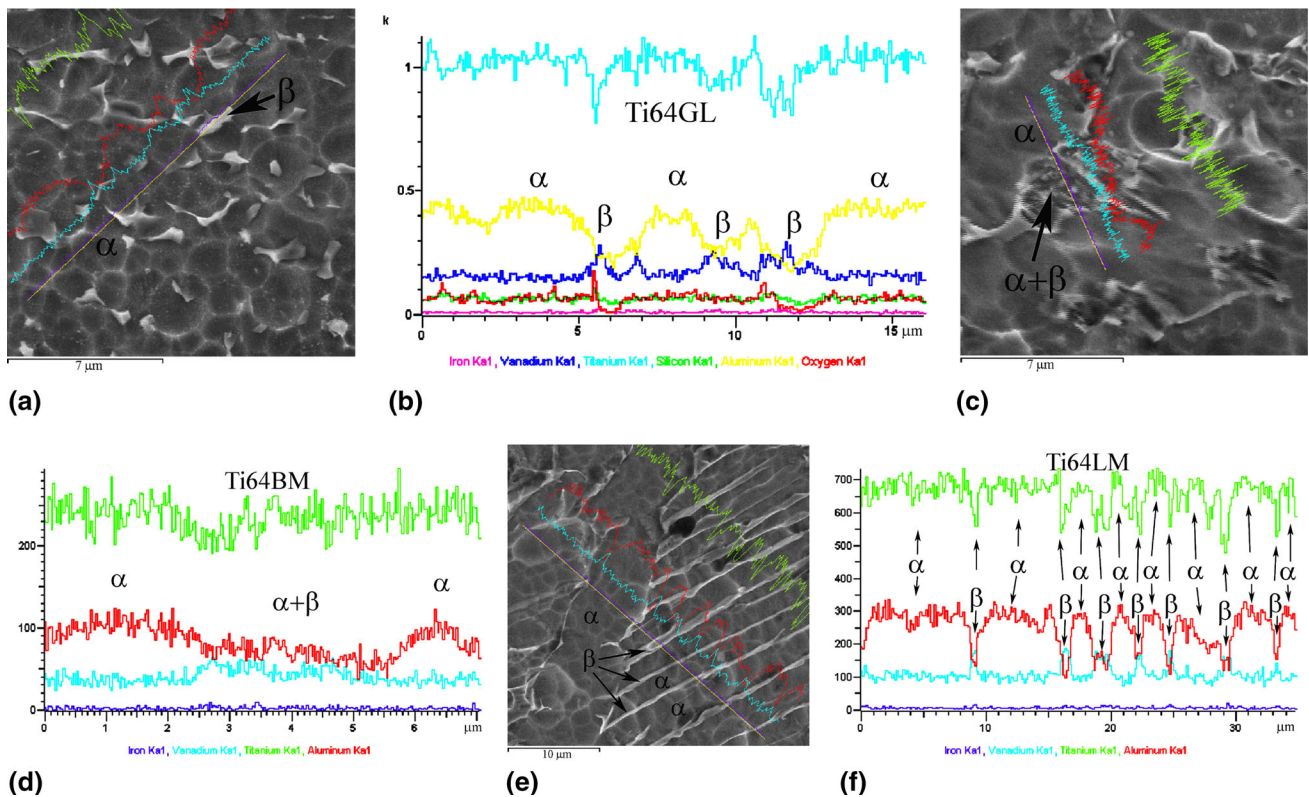


Fig. 13 Chemical composition measured on polished specimens in initial (not tested) state: (a, b) Ti64GL, (c, d) Ti64BM and (e, f) Ti64LM. (a, c, e) correspondence between microstructures and concentration profiles, (b, d, f) concentration profiles. SEM, EDS

it is very close to the composition of β -phase (p 6 in Table 3), whereas in p 54 (Table 2)—to the α -phase (p 5 in Table 3). At the same time, the majority of both brittle and ductile zones have chemical composition rather similar to the nominal content of alloying elements in this alloy, which allows to assume the same general character of fracture at the α/β interphase boundaries. Under these conditions, the previously mentioned special cases of increased content of alloying elements can be explained by local brittle fracture of specimens, which occurred by tearing along the edge of the α/β interfaces, thereby “baring” the surface of α - or β -phase.

3.3 Metastable β Alloy LCB in Annealed Two-Phase $\alpha + \beta$ Condition

This alloy was subjected to a detailed study in previous works (Ref 10, 11) in single-phase metastable β condition and two-phase aged $\alpha + \beta$ condition; the latter was characterized by high strength (because of very fine α -precipitates inside β -grains) and low ductility. Present material has rather similar to aged fine-grained [as a result of special rapid heat treatment (Ref 11)] microstructure, namely relatively small β -grains with boundaries covered by lamellar α -phase and α -phase precipitates inside, but due to higher temperature of annealing α -particles were coarser (Fig. 1f), which resulted in lower strength and much higher ductility (Fig. 14). The influence of strain rate on the mechanical properties is absolutely typical for all studied alloys and microstructural conditions—strength became higher and elongation lower at higher strain rates. At the same time, it is necessary to mention the specific features of this alloy. First of all, all stress-strain curves have yield tooth

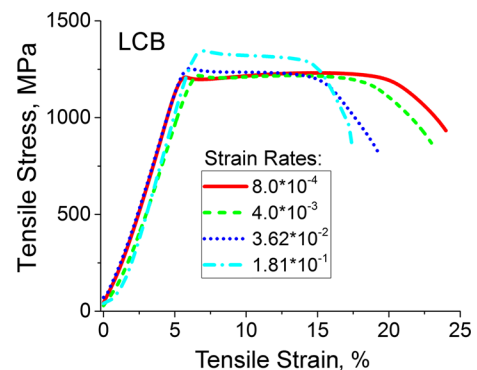


Fig. 14 Typical engineering stress-strain curves of LCB in annealed $\alpha + \beta$ state tested with different strain rates

(yield drop) that is usually associated with the intensification of the process of formation of new dislocations or their escaping from Cottrell atmospheres which hinder their sliding (Ref 21, 22). Moreover, the elevation of strain rate resulted in a change in inclination of uniform deformation region from positive to negative one. The last effect was discussed earlier for aged microstructural conditions of this alloy (Ref 11): It was suggested that at lower strain rates tension is controlled by deformation in the β phase, whereas at higher strain rates plastic flow is governed by processes in the α phase.

The TT dependencies on strain rate for LCB are presented in Fig. 15. Total TT decreased with strain rate, like in other microstructural conditions of this alloy, as well as in other

titanium alloys of metastable β -class (Ref 10-12). In this case, the main input into TT values is provided by uniform plastic deformation to necking that hardly varies with straining rate increase, while localized plastic deformation after necking comes down. It can be mentioned that in all other studied β -alloys the dependencies of these constituents on strain rate were opposite.

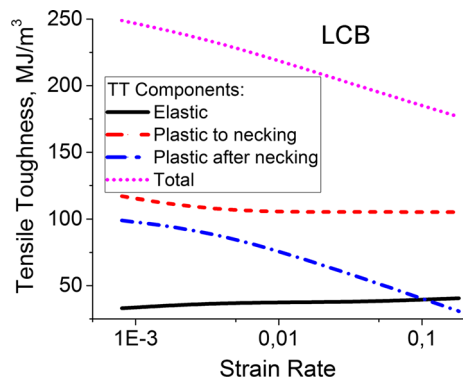


Fig. 15 Tensile toughness of LCB in annealed $\alpha + \beta$ state tested with different strain rates

Typical examples of fracture surfaces of LCB specimens tested with different strain rates are presented in Fig. 16. First of all, it should be mentioned that the general character of fracture for all strain rates investigated was ductile and the diameter of dimples (2-5 μm) is comparable with average size of β -grains (Fig. 1f; p 6 in Table 1). At the same time, it is clearly seen at smaller magnifications (Fig. 16a, c and e) that fine dimples form some ensembles, which, as can be assumed, may be related to close crystallographic orientations of β -grains in these areas. At higher magnifications, the holes in the bottom of dimples are observed, which indicates the formation of voids near the fracture surface (Fig. 16b, d and f).

Details of microstructure of the alloy after deformation are shown in Fig. 17. Both α - and β -phases had increased density of dislocations (Fig. 17a), which was approximately similar in both phases. This fact means that both phases are characterized by rather equal strength, or it took place due to relatively fine size of α -lathes and β -interlayers. At higher magnifications, in some α -particles separate stacking faults were found (Fig. 17b).

Microstructure of LCB in the region near fracture surface is shown in Fig. 18. A comparison of Fig. 1f and 18 shows that the majority of α -lamellae of both types (coarser along β -grain boundaries and finer inside grains) tilted in the direction of applied stress and plastic flow. Contrary to Ti-6-4 alloy, the intragrain $\alpha + \beta$ microstructure in LCB material was much finer

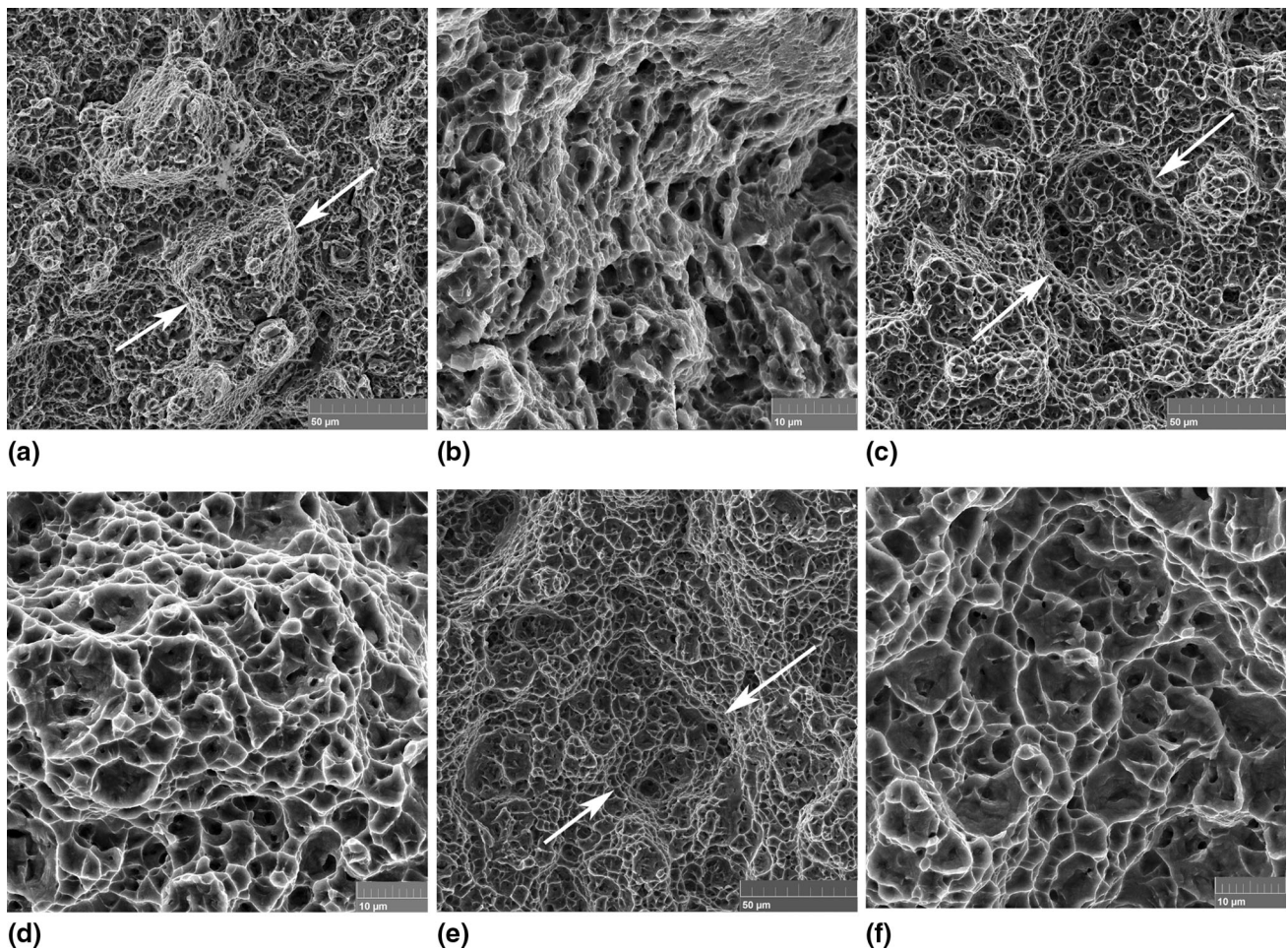


Fig. 16 Typical fracture surfaces of TIMETAL-LCB in annealed $\alpha + \beta$ state tested with strain rates: (a, b) 8.00×10^{-4} , (c, d) 3.62×10^{-2} and (e, f) 1.82×10^{-1} . Arrows in Fig. 16(a), (c), and (e) show the ensembles of dimples. SEM

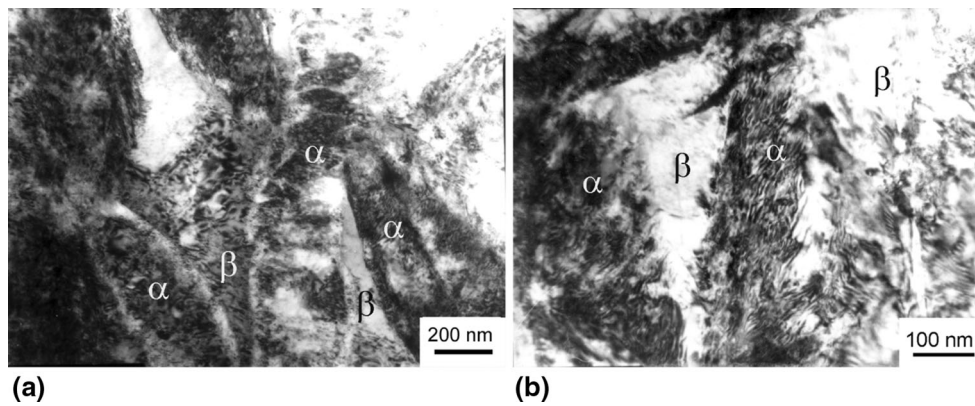


Fig. 17 Typical TEM images of LCB specimens tensile tested with rate 1.81×10^{-1} near the fracture surface. TEM

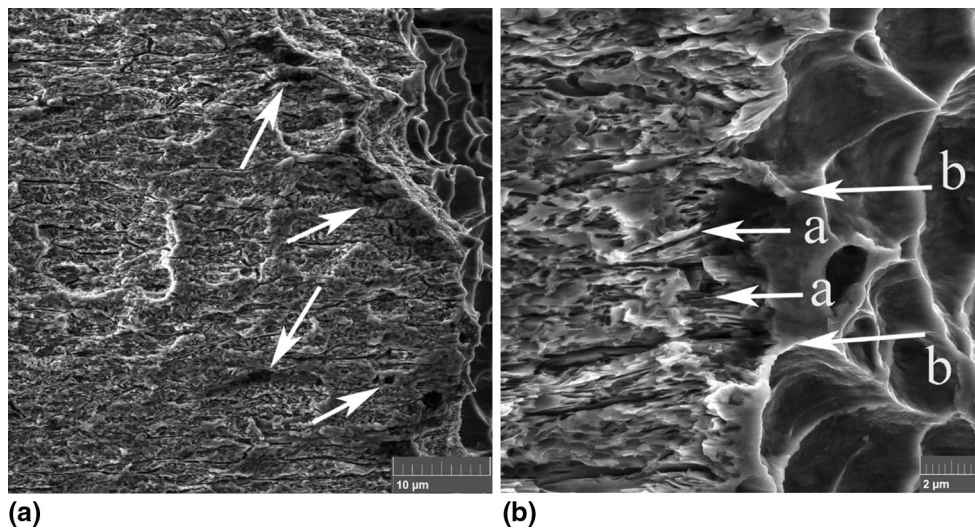


Fig. 18 Typical microstructure of LCB specimens polished in longitudinal direction under the fracture surface (strain rate 1.81×10^{-1}): (a) arrows indicate voids under the fracture surface; (b) “a” arrows show tips of fine α -lamellae at which voids formed and “b” arrows show the correspondence between coarser grain boundary α -lamellae and dimple edges

(compare Fig. 1c and d with f); therefore, the voids in tested specimens under fracture surface were finer as well (Fig. 18a). A higher-magnification image allows assuming that the smallest voids were initiated at the tips of fine intragrain α -lamellae (“a” arrows in Fig. 18b), while the edges of dimples on the fracture surface look like extensions of β -grain boundaries, covered by somewhat coarser α -lamellae (“b” arrows in Fig. 18b). In (Ref 12), it was supposed that thin layers enriched in β -stabilizers are formed near β -grain boundaries in other titanium metastable β -alloys in aged ($\alpha + \beta$) condition, and these embrittled layers were considered as the weakest link that causes fracture upon tension. Similar situation is possible in the present material. Unfortunately, too fine intragrain microstructure did not allow to reveal correctly the distribution of elements in the phase constituents (Fig. 19). Nevertheless, the periodical fluctuations of titanium content allow to assume that higher Ti concentrations correspond to α -phase, whereas lower Ti concentrations may be associated with β -phase (Fig. 19b). Indeed, more precise measurements of local composition showed essential difference in alloying elements content in α - and β -phases (Table 4), but these results are rather facultative because of significant error due to fine microstructure.

The results of chemical analysis of fracture surfaces are listed in Table 5. First of all, it should be noted that chemical composition on the surface of different dimples varies in a very wide range—from very low concentrations of all alloying elements (aluminum, molybdenum and iron), p 6, 12 and 15, to comparatively high concentrations of both β - and α -stabilizing elements, p 3, 8, 9 and 13. Therefore, it can be assumed that failure is likely to occur between enriched and depleted layers present near the grain boundary α -phase. In general, the mechanism of fracture is similar to the cases of Ti64BM and Ti64LM, namely—the pores nucleated near the tips of intragranular α -phase plates (needles), then grew, merged and reached the grain boundary α -lamellae, forming fracture dimples.

4. Comparison of the Alloys

A comparison of tensile toughness dependencies on strain rate for all studied alloys and microstructural states is shown in Fig. 20, where some data for other titanium metastable β -alloys

from the previous works (Ref 11, 12) are added. First of all, it is worthwhile to underline that for all materials and microstructures the TT level significantly drops with strain rate, except Ti64GL material. The last fact is very unusual, but can be used for explanation of the result obtained by J. Fanning (Ref 6) who

found out that Ti-6-4 alloy has the best antiballistic properties among a wide range of commercial titanium alloys. However, as can be seen from a comparison of curves ##3, 4 and 5, the low sensitivity of this alloy to strain rate is peculiar to globular condition only, whereas bimodal and lamellar microstructures

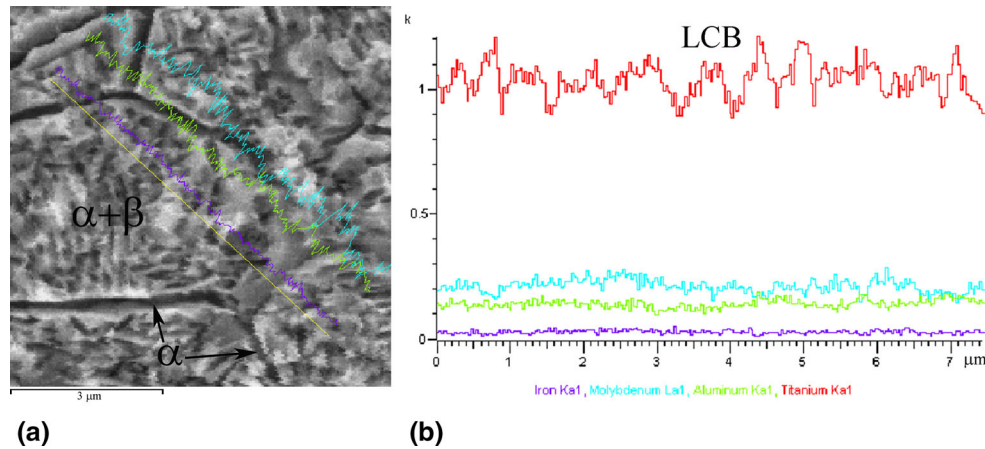


Fig. 19 Chemical composition of polished LCB sample (not tested). (a) Correspondence between microstructure and concentration profiles, (b) concentration profiles

Table 4 Local chemical composition of TIMETAL-LCB in initial annealed $\alpha + \beta$ state

##	Average chemical composition, wt.%			Phase
	Al	Mo	Fe	
1	1.68	(4.15)	1.23	α
2	0.75	(9.53)	6.08	β

Table 5 Local chemical compositions on fracture surface of TIMETAL-LCB alloy after annealing (two-phase $\alpha + \beta$ state)

##	Strain rate	Chemical composition, wt.%			Location
		Al	Mo	Fe	
1	1 mm/min (8.00×10^{-4})	0.43	3.76	3.42	Ductile
2		1.41	7.93	4.32	
3		1.54	9.34	5.21	
4		1.10	7.42	4.23	
5		1.39	7.16	3.87	
6		0.29	2.15	2.27	
Average	50 mm/min (3.62×10^{-2})	1.03	6.30	3.89	Ductile
7		0.88	5.44	3.82	
8		1.38	8.24	5.16	
9		1.93	7.85	4.38	
10		0.70	1.69	1.43	
11		0.54	1.80	1.52	
12	0.17	1.73	2.69	Ductile	
Average	250 mm/min (1.81×10^{-1})	0.94	4.46		3.17
13		1.22	7.06		4.72
14		0.64	1.91		1.13
15		0.53	0.84		0.93
16		1.22	7.08		3.92
17		0.65	3.60	2.64	
18	1.16	5.91	3.75	Ductile	
Average	0.91	4.59	3.01		

have common TT dependencies on strain rate. It is also noteworthy that Ti64LM condition is characterized by the worst TT level (curve #4) which is even lower than that of the c.p.Ti (curves ##1 and 2) which has much lower strength. Ti64BM

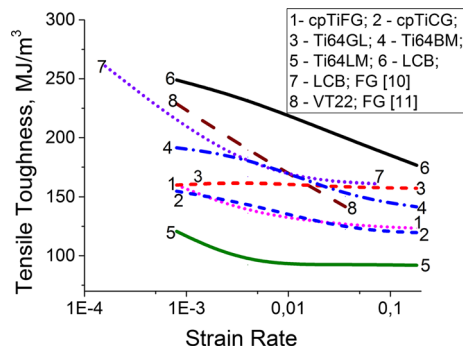


Fig. 20 Comparison of total tensile toughness of studied materials (1-6) and two earlier investigated titanium alloys of β -metastable type in a single-phase fine-grained β -state [7 LCB (Ref 11) and 8 VT22 (Ref 12)]

condition has higher TT level as compared to Ti64GL condition at tension with slow rates, whereas at faster deformation the situation is reversed (compare curves ##3 and 4). The results for Ti64GL condition at high strain rates look even better in comparison with the best results obtained for high-strength metastable β -alloys LCB and VT22 in a fine-grained single-phase β -state. Only LCB alloy in two-phase $\alpha + \beta$ condition investigated in the present study has higher TT than Ti64GL at all applied strain rates, but the strain rate dependencies for these two materials are principally different, so it is likely that at faster deformation any superiority of LCB can disappear. Summarizing all the above, we can assume that the specific behavior of Ti-6-4 alloy can be explained by its microstructure only and may be associated with relatively fine size of primary α -phase globules, large amount of high-angle α/α boundaries and rather small amount of α/β interfaces. Better antiballistic properties of globular type microstructure of Ti-6-4 alloy in comparison with lamellar one were also established in (Ref 23, 24).

The dependencies of TT and elongation on UTS for the alloys studied in this work and two previous ones are presented in Fig. 21. It should be stressed that for all materials these

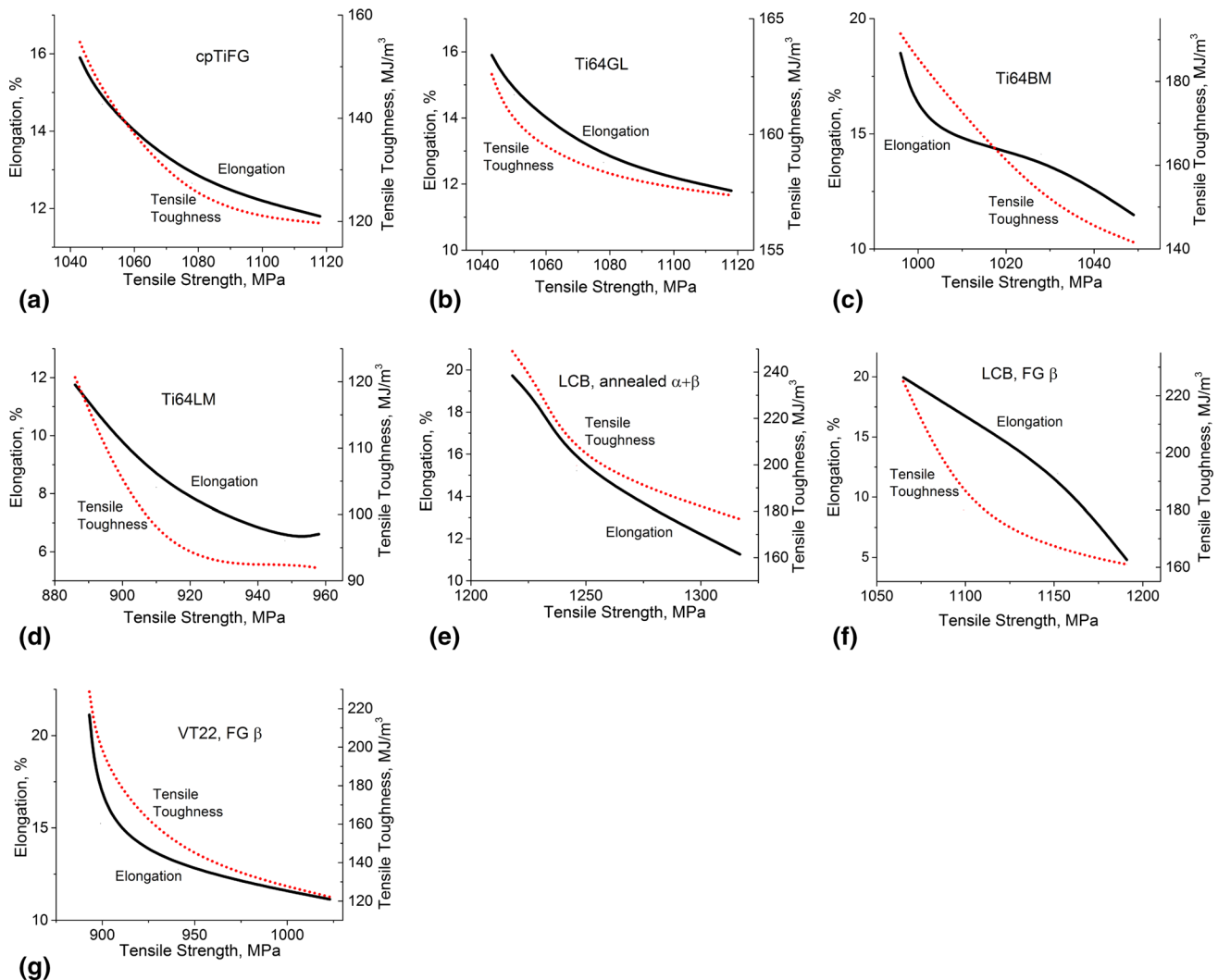


Fig. 21 Dependencies of elongation and tensile toughness on ultimate tensile strength for: (a) cpTiFG, (b) Ti64GL, (c) Ti64BM, (d) Ti64LM, (e) LCB, (f) LCB in fine-grained single-phase β condition (Ref 11) and (g) VT22 in fine-grained single-phase β condition (Ref 12)

Table 6 Results of experiments on ultrasound propagation in Ti-6-4 samples with different microstructures

Specimens	Sound velocity, longitudinal $\langle v_l \rangle$ (m/s)	Sound velocity, transverse $\langle v_t \rangle$ (m/s)	Attenuation coefficient, longitudinal α_l (db/ μ s)	Attenuation coefficient, transverse α_t (db/ μ s)	Young Modulus, E (GPa)	Shift modulus, G (GPa)	Compression modulus, B (GPa)	B/G (Relative units)	Poisson's coefficient η (Relative units)
Ti64GL	6092.2	3143.4	1.52	1.18	115.1	43.64	105.7	2.42	0.319
Ti64BM	6115.1	3157.45	1.89	1.33	116.0	44.01	106.4	2.42	0.318
Ti64LM	6175.7	3251.7	2.83	2.79	122.1	46.68	106.1	2.27	0.308

dependences have similar character, and the differences between alloys and microstructural states are minor. In general, this allows to conclude that the main contribution to the tensile toughness for these alloys and strain rates is provided by uniform plastic deformation. For the cpTiFG, both TT and elongation curves look rather similar, and the ratio between these two parameters equals 10 (Fig. 21a). For all three microstructural states of Ti-6-4 alloy, there are good correspondences between the dependencies of TT and elongation on UTS (Fig. 21b, c and d); for Ti64GL and Ti64BM materials, the ratio between TT and elongation is about 11-12, while for Ti64LM it varies from 10 to 13.4 with increase in strength (i.e., with increase in strain rate). For studied in this work LCB (in annealed two-phase $\alpha + \beta$ state), the ratio between these characteristics is 12 (Fig. 21e) within the whole range of strain rates investigated. At the same time, for the single-phase β -condition of the same alloy the TT and elongation change with increase in UTS (or strain rate) in different ways (Fig. 21f). Contrary to all other cases, in this one the ratio between these two characteristics changes with UTS (or strain rate) in a very wide range, namely from 11.3 to 32. Another titanium metastable β -alloy, VT22, in single-phase β -condition has common curves (Fig. 21h), and the ratio between TT and elongation is about 11 for all studied strain rates. The significant difference between these two β -alloys can be explained by the earlier found difference in their deformation accommodation modes (Ref 25), as well as the noticeable difference in UTS.

4.1 Influence of Microstructure and Phase Composition

4.1.1 cpTi. As can be concluded from the analysis of experimental data, single-phase h.c.p. α -titanium at all studied strain rates deforms uniformly, and local deformation occurs at the last stages immediately before fracture. The main role in the formation of voids and main cracks is played not by α -phase grains, but by the elements of intragrain substructure formed on plastic flow during uniform deformation, and this substructure forms very easily throughout the whole volume of the metal even at the highest strain rates used in this work. In the alloy with coarse grains, main cracks partially propagate along the grain boundaries at high strain rates only.

4.1.2 Ti64GL. Taking into account all the above, it can be concluded that in the Ti64GL specimens the voids form at the α/β interfaces (Fig. 11b), and first of all at the triple junctions. Since the amount of such interfaces is relatively restricted (Fig. 1c), and both phases are rather ductile (Ref 2, 14), probably this can explain the weak dependence of TT on strain rate. Generally, the process of fracture evidently develops through the merging of neighboring voids which finally form the fracture dimples (Fig. 8a, b, e and h). This leads to the fact that the final size of the dimples is equal to the distance between the two closest α/β interfaces and meets the size of the primary α -globules (or few neighboring globules, which have no β -particles between them).

4.1.3 Ti64BM. In this microstructure, the voids and cracks are initiated in the regions of β -transformed mixture of $\alpha + \beta$ phases (Fig. 1d), and first of all—at stronger small lamellar α -particles, namely at their tips (Fig. 13c and d). During deformation, these α -particles tilt in the direction of applied load and plastic flow of metal. Obviously, their influence gets stronger with increase in strain rate, resulting

in the decrease in TT with strain rate. The fracture process occurs as mentioned above—by merging of neighboring voids; due to comparatively uniform distance between the neighboring β -transformed regions, the size of dimples corresponds to the diameter of primary α -globules, or ensembles of few neighboring globules not divided by $\alpha + \beta$ regions.

4.1.4 Ti64LM. In this case, the tips of α -lamellae play the role of void initiation sites (Fig. 13f). Then, the neighboring voids merge to form an initial crack, which looks on fracture surface as ductile dimples (Fig. 8d, g and j). If during its growth this crack reaches the α -lamellae covering β -grain boundary, it spreads quickly through it (Fig. 13e), forming cleavage facets on the fracture surface (Fig. 8d, g and j).

In order to identify the physical nature of the influence of microstructure on the mechanical behavior of Ti-6-4 alloy, first of all it is necessary to take into account that these properties are controlled by dislocation motion, which in turn can slide with a velocity up to speed of sound (Ref 22, 23). Therefore, we measured the speed of sound and attenuation coefficients and calculated all relevant parameters in Ti-6-4 material with all three microstructures. As shown in Table 6, both longitudinal and transverse speeds of sound slightly increase in the order Ti64GL \rightarrow Ti64BM \rightarrow Ti64LM; similar changes are also seen for all modules and Poisson's ratio. At the same time, the attenuation coefficients in the lamellar microstructure are almost two times higher as compared to two other microstructures. This allows to conclude that the higher number of α/β interphase boundaries (contrary to predominantly α/α boundaries in Ti64GL and Ti64BM materials) caused intensive dispersion and absorption of sound. In our case, this obviously means more hindered motion of dislocations, which resulted in lower mechanical properties of this microstructure, including tensile toughness. In other words, the presence of comparatively large number of planar interphase boundaries (2D) leads to more efficient phonon scattering in comparison with a small number of 3D boundaries in a globular microstructure. It should be noted that upon realization of diffusion processes, the reverse situation takes place; namely, in globular microstructures all diffusion processes proceed approximately $\sqrt{3}$ times faster than in the lamellar one (Ref 26, 27).

4.1.5 LCB. Apparently, in this alloy the voids were also initiated at small intragrain lamellar α -particles, and these acicular particles also tilted in the direction of applied load and plastic flow of metal (Fig. 15). However, as shown in Fig. 15(b), fine voids in neighboring α -particles merge until they reach the closest coarse α -plates at β -grain boundary, finally forming on the fracture surface relatively coarse dimples (Fig. 10). These dimples are somewhat smaller than the average β -grain size, because during deformation the grains elongate in tension direction and get narrower in transverse one.

4.2 Influence of Strain Rate

In general, in all alloys and microstructural conditions increase in strain rate resulted in a reduction in uniform plastic deformation stage (plastic flow to necking). At the same time, faster tension makes thinner layer under the fracture surface where pores nucleate. In Ti-6-4 alloy with all structural states and in LCB, faster tension causes in appearance of yield tooth (Fig. 8b and 14). As it was shown in (Ref 28, 29), stress drop after start of yielding is associated with abrupt increase in the density of mobile dislocations (e.g., due to their generation at grain boundaries) and usually takes place at high-temperature

deformation. This phenomenon is also inherent to single β -phase condition strained at room temperature at relatively high strain rates (Ref 10-12, 30), whereas in two-phase $\alpha + \beta$ state the presence of secondary α -phase and large number of α/β interphase boundaries inside β -grains play more important role in the mechanical behavior of material. Some softening (the absence of strain hardening) of material was observed in Ti-6-4 and especially in LCB strained with rates above 3.62×10^{-2} . For the first alloy, the same effect of softening on tension at room temperature was observed in Ti-6-4 alloy with microcrystalline and submicrocrystalline structures (Ref 31). According to the works (Ref 32, 33), this behavior is usually attributed to plastic instability originating from the lack of an effective hardening mechanism; this instability appears as either formation of shear bands or “early” necking. In our case in Ti64BM, Ti64LM and LCB materials, this led to the localization of plastic deformation near some fine stress concentrators inside the materials—tips of fine α -phase particles. Obviously, the tendency of deformation localization with increase in deformation (strain or any other kind) rate is rather common, and beyond some critical level (Ref 34), it leads to the transition from usual plastic deformation (associated with dislocations, twinning, crystal lattice rotation, etc.) to the formation of adiabatic shear bands (Ref 35). However, even in this case some superiority of globular microstructure over lamellar one was found for Ti-6-4 alloy (Ref 23, 24): The material with globular microstructure had better ballistic properties as compared to lamellar one for the same testing conditions.

The study of influence of strain rate on the mechanism of pore formation and rupture initiation allows to conclude that faster tension causes higher localization of deformation defects near grain/subgrain boundaries (in single α - or β -materials) or α/β interphase boundaries (in two-phase ones) and, as a result, faster appearance of voids and their coalescence into initial cracks (Ref 30).

5. Conclusions

1. All studied materials showed a decrease in tensile toughness (deformation energy) with strain rate that apparently was caused by a decrease in ability to uniform plastic deformation, which is reflected primarily in the reduction in relative elongation. In c.p.Ti at all studied strain rates, the main part of plastic deformation realized via uniform elongation that led to a high density of intragrain defects, which acted as nucleation sites for voids and cracks; general character of fracture was ductile. In c.p.Ti with coarse-grained microstructure (diameter of α -grains not less than 200 μm), the secondary cracks developed through separate grain boundaries at strain rates higher than 3.62×10^{-2} .
2. In Ti-6-4 and LCB alloys in two-phase $\alpha + \beta$ conditions, the uniform plastic deformation also made the main input into tensile toughness at all strain rates applied. At the same time, Ti-6-4 alloy with globular microstructure had the lowest sensitivity of tensile toughness to strain rate, apparently due to the fine globular microstructure of α -phase, small amount of relatively soft second β -phase and thus prevalence of α/α -grain boundaries over the α/β interphase boundaries. However, exactly α/β interphase boundaries are places of voids nucleation and formation

- of cracks. In the first alloy, the higher number of α/β interphase boundaries in bimodal microstructure resulted in a higher sensitivity to strain rate, and their 100% presence in lamellar condition led to the lowest level of tensile toughness. In both cases, the voids and cracks were initiated by α -phase particles at: (1) tips of fine intragrain needles in bimodal microstructure and (2) tips of coarse α lamellae further propagating along the top of the $\alpha + \beta$ packet in lamellar one. In the first case, general character of fracture remains ductile (like in case of globular microstructure), while in lamellar microstructure fracture begins ductile, but reaching β -grain boundary cracks propagates along covering grain boundary coarse α lamellae forming brittle cleavage facets. Basing on the results of speed of sound and attenuation coefficients measurements, it was supposed that the higher number of α/β interphase boundaries in lamellar microstructure hindered motion of dislocations causing in worse mechanical properties.
- In LCB alloy annealed for two-phase $\alpha + \beta$ condition, the voids and cracks were initiated also at tips of intragrain (finer than covering β -grain boundaries) α -lamellae. Despite relatively higher than in Ti-6-4 general level of strength, but due to rather small size of β -grains, and thus better ductility, fracture in this material was also completely ductile. Generally, Ti-6-4 with bimodal and lamellar microstructures, as well as LCB alloy having two-phase $\alpha + \beta$ microstructure, has similar fracture mechanism: Pores nucleated near the tips of intragranular α -phase plates (needles), then grew, merged and reached next $\alpha + \beta$ region (in Ti-6-4 with globular microstructure) or grain boundary α -lamellas (in two other cases), forming fracture dimples.
 - Comparison of difference in microstructure, chemical and phase composition alloys allowed to conclude that the better tensile toughness at all strain rates applied had annealed for two-phase $\alpha + \beta$ condition LCB. At the same time, only Ti-6-4 with globular microstructure was characterized by very low sensitivity of tensile toughness to strain rate.

Acknowledgments

Parts of this work were done in frames of the Projects ## III-09-13 and 01-07-16 funded by National Academy of Sciences of Ukraine. Authors would like to thank Dr. O.I. Zaporozhets for supersonic measurements and Mr. M.A. Skoryk (both from G.V. Kurdyumov Institute for Metal Physics, NAS of Ukraine) for help in SEM studies.

Conflict of Interest

The authors declare that they have no conflict of interest.

References

- Advances in the Products and Technology of Titanium Alloys Processing, *Advances in Science and Technology of Titanium Alloys Processing, 1996 TMS Annual Meeting*, 4-8 February 1996, Anaheim, CA
- G. Luetjering and J.C. Williams, *Titanium*, 2nd ed., Springer, Berlin, 2007
- R.R. Boyer and R.D. Briggs, The use of β Titanium Alloys in the Aerospace Industry, *J. Mater. Eng. Perform.*, 2005, **14**, p 681–685
- <http://boom.aero/>
- US Patent No.: 9,079,661B2; Ultra-Rapid Air Vehicle and Related Method for Aerial Locomotion
- J. Fanning, Military Application for β Titanium Alloys, *J. Mater. Eng. Perform.*, 2005, **14**, p 686–690
- J.S. Montgomery and M.G.Y. Wells, Titanium Armor Applications in Combat Vehicles, *JOM*, 2001, **4**, p 29–32
- N. Stefansson, I. Weiss, A.J. Hutt et al., Work Hardening in Beta Titanium Alloys, *Titanium'95: Science and Technology*, Vol 2, P.A. Blenkinsop, W.J. Evans, H.M. Flower, Ed., The University Press, Cambridge, 1996, p 980–987
- A. Bhattacharjee, P. Ghosal, A.K. Gogia et al., Room Temperature Plastic Flow Behaviour of Ti-6.8Mo-4.5Fe-1.5Al and Ti-10V-4.5Fe-1.5Al: Effect of Grain Size and Strain Rate, *Mater. Sci. Eng. A*, 2007, **452-453**, p 219–227
- P.E. Markovsky, V.I. Bondarchuk, and YuV Matviychuk, Influence of Grain Size and Crystallographic Texture on Mechanical Behavior of TIMETAL-LCB in Metastable β -Condition, *Mater. Sci. Eng.*, 2013, **A559**, p 782–789
- P.E. Markovsky, V.I. Bondarchuk, and O. Gerasimchuk, Influence of Grain Size, Aging Conditions and Tension Rate on Mechanical Behavior of Titanium Low-Cost Metastable Beta-Alloy in Thermally Hardened Condition, *Mater. Sci. Eng.*, 2015, **A645**, p 150–162
- P.E. Markovsky, V.I. Bondarchuk, O.V. Shepotinnyk, and I.M. Gavrysh, Influence of Phase Composition and Microstructure on Mechanical Behavior of Ti-3Al-4.5Fe-7.2Cr and VT22 Titanium Metastable β Alloys on Tension with Different Rates, *Metallofiz. Noveishie Tekhnol.*, 2016, **38**, p 1057–1074
- J.R. Davis, Ed., *Tensile Testing*, 2nd ed., ASM International, Materials Park, 2004
- G. Lutjering, Influence of Processing on Microstructure and Mechanical Properties of ($\alpha + \beta$) Titanium Alloys, *Mater. Sci. Eng.*, 1998, **A243**, p 32–45
- V.F. Moiseev, Effective Strain Hardening Rate of the Metals, *Metallofiz. Noveishie Tekhnol.*, 2001, **23**, p 387–399 (in Russian)
- G. Sukumar, B. Bhav Singh, A. Bhattacharjee, K. Siva Kumar, and A.K. Gogia, Ballistic Impact Behavior of β -CEZ Ti Alloy Against 7.62 mm Armor Piercing Projectiles, *Int. J. Impact Eng.*, 2013, **54**, p 149–160
- E. Wielewski, G.J. Appleby-Thomas, P.J. Hazell, and A. Hameed, An Experimental Investigation into the Micro-mechanics of Spall Initiation and Propagation in Ti-6Al-4V During Shock Loading, *Mater. Sci. Eng.*, 2013, **A578**, p 331–339
- X. Boidin, P. Chevrier, J.R. Klepaczko, and H. Sabar, Identification of Damage Mechanism and Validation of a Fracture Model Based on Mesoscale Approach in Spalling Of Titanium Alloy, *Int. J. Solids Struct.*, 2006, **43**, p 4595–4615
- K. Sun, X. Yu, Ch Tan, H. Ma, F. Wang, and H. Cai, Effect of Microstructure on Adiabatic Shear Band Bifurcation in Ti-6Al-4V Alloys Under Ballistic Impact, *Mater. Sci. Eng. A*, 2014, **595**, p 247–256
- J. Goldstein, D.E. Newbury, D.C. Joy, C.E. Lyman, P. Echlin, E. Lifshin, L. Sawyer, and J.R. Michael, *Scanning Electron Microscopy and X-ray Microanalysis*, 3rd ed., Springer, Berlin, 2003
- X.J.P. Hirth and J. Lothe, *The Theory of Dislocations*, Krieger Pub Co, Malabar, 1992
- F.P. Beer, E.R. Johnston, J.T. DeWolf, and D.F. Mazurek, *Mechanics of Materials*, 7th ed., McGraw-Hill, New York, 2015
- Chao Zheng, Fuchi Wang, Xingwang Cheng et al., Failure Mechanisms in Ballistic Performance of Ti-6Al4V Targets Having Equiaxed and Lamellar Microstructures, *Int. J. Impact Eng.*, 2015, **85**, p 161–169
- M.S. Burins, J.S. Hansen, J.I. Paige, and P.C. Turner, *The Effect of Thermo-mechanical Processing on the Ballistic Limit Velocity of Extra Low Interstitial Titanium Alloy Ti-6Al-4V*, Army Research Laboratory Report ARL-MR-486, July 2000
- O.P. Karasevska, O.M. Ivasishin, S.L. Semiatin, and YuV Matviychuk, Deformation Behavior of Beta-Titanium Alloys, *Mater. Sci. Eng.*, 2003, **A354**, p 121–132
- C. Zener, Theory of Growth of Spherical Precipitate from Solid Solution, *J. Appl. Phys.*, 1949, **20(9)**, p 950–953

27. V.N. Gridnev, O.M. Ivasishin, and P.E. Markovsky, Influence of Heating Rate on the Temperature of the $(\alpha + \beta) \rightarrow \beta$ —Transformation of Titanium Alloys, *Met. Sci. Heat Treat.*, 1985, **27**(1), p 43–48
28. I. Philippart and H.J. Rack, High Temperature, High Strain Deformation Behavior of Ti-6.8Mo-4.5Fe-1.5Al, *Mater. Sci. Eng. A*, 1998, **254**, p 253–267
29. I. Philippart and H.J. Rack, High Temperature Dynamic Yielding in Metastable Ti-6.8Mo-4.5F-1.5Al, *Mater. Sci. Eng. A*, 1998, **243**, p 196–200
30. M.A. Meyers and K.K. Chawla, *Mechanical Behavior of Materials*, Cambridge University Press, Cambridge, 2009
31. S. Zherebtsov, G. Salishchev, R. Galejev, and K. Maekawa, Mechanical Properties of Ti-6Al-4V Titanium Alloy with Submicrocrystalline Structure Produced by Severe Plastic Deformation, *Mater. Trans. Jpn. Inst. Met.*, 2005, **46**(9), p 2020–2025
32. K.S. Kumar, H. Van Swygenhoven, and S. Suresh, Mechanical Behavior of Nanocrystalline Metals and Alloys, *Acta Mater.*, 2003, **51**, p 5743–5774
33. A. Vinogradov, S. Hashimoto, and V.I. Kopylov, Enhanced Strength and Fatigue Life of Ultra-Fine Grain Fe-36Ni Invar Alloy, *Mater. Sci. Eng. A*, 2003, **355**, p 277–285
34. O.B. Naimark and M.A. Sokovnikov, About Adiabatic Shear Mechanism on High-Rate Loading of Materials, *Math. Model. Syst. Process.*, 1995, **3**, p 71–76 (in Russian)
35. B. Wang, J. Sun, E.N. Hahn, and X. Wang, Shear Localization and its Related Microstructure Mechanism in a Fine-Grain-Sized Near-Beta Ti Alloy, *J. Mater. Eng. Perform.*, 2015, **24**, p 477–483